Specific and fuzzy interactions cooperate in modulating protein half-life

Rashmi Sharma[1§], Máté Demény[1§], Viktor Ambrus[1], Sándor Balázs Király[2], Tibor Kurtán[2], Pietro Gatti-Lafranconi[3], Monika Fuxreiter[1]*

[1] *MTA-DE Laboratory of Protein Dynamics, Department of Biochemistry and Molecular Biology, University of Debrecen, Debrecen, Hungary*
[2] *Department of Organic Chemistry, University of Debrecen, Debrecen, Hungary*
[3] *Department of Biochemistry, University of Cambridge, UK*

Corresponding email: fmoni@med.unideb.hu

[§] these authors contributed equally to the work

Keywords: protein degradation, 20S proteasome, AP-1 complex, fuzzy complex, nanny model

Abstract

Protein degradation is critical for maintaining cellular homeostasis. The 20S proteasome is selective for unfolded, extended polypeptide chains without ubiquitin tags. Sequestration of such segments by protein partners, however, may provide a regulatory mechanism. Here we used the AP-1 complex to study how c-Fos turnover is controlled by interactions with c-Jun. We show that heterodimerization with c-Jun increases c-Fos half-life. Mutations affecting specific contact sites (L165V, L172V) or charge separation (E175D, E189D, K190R) with c-Jun both modulate c-Fos turnover, proportionally to their impact on binding affinity. The fuzzy tail beyond the structured b-HLH/ZIP domain (~165 residues) also contributes to the stabilization of the AP-1 complex, removal of which decreases c-Fos half-life. Thus, protein turnover by 20S proteasome is fine-tuned by both specific and fuzzy interactions, consistently with the previously proposed 'nanny' model.

Introduction

Precise protein quality control is crucial for all cellular processes. The proteasome system is responsible for selective degradation of proteins to eliminate damaged, misfunctional or foreign sequences and tightly regulate protein turnover [1, 2]. Alterations in half-life affects proliferation, apoptosis, DNA repair, immune and stress response and aberrant protein homeostasis is associated with developmental problems, cancer and neurodegenerative pathologies [3-5]. The 26S proteasome [6] consists of the 20S catalytic core for proteolysis of unfolded segments [7-9], and the 19S regulatory particle(s) to recognize substrates with poly-ubiquitin (Ub) tags [10, 11]. The unstructured initiation sites exhibit biased amino acid compositions, which modulate the affinity for the proteasome [12]. Certain sequence signatures (eg. low-complexity motifs) however, may increase stability of unfolded segments and selectively inhibit proteolysis [13, 14].

Proteomic analysis of the 20S substrates revealed the enrichment of segments, which lack a well-defined tertiary structure in their native states [15]. Intrinsically disordered (ID) regions could be degraded by 'default' via the 20S core particle, in accord with earlier proposals [16]. Indeed, proteins possessing long (≥ 30 residues) intrinsically disordered regions exhibit shorter half-life than those with shorter ID regions [17]. This presents a challenge for selective degradation: how to distinguish between non-functional, unfolded segments and exposed, dynamic, regulatory regions? Early observations indicated that turnover of inherently unstable proteins (e.g. ornithine decarboxylase) could be inhibited by complex formation with NAD(P)H quinone oxidoreductase 1 (NQO1) [18], which exerts a negative feedback for the 20S proteasome [19]. NQO1 is a ubiquitous enzyme, which can also stabilize p53 and p73α transcription factors to inhibit degradation [16].

Generalization of these observations lead to the proposal, that protein interactions might shield exposed, disordered regions and make them inaccessible to the 20S catalytic machinery [20]. The survival of proteins with inherently unstable regions thus depends on the availability of their interacting partners ('nannies') [20]. In accord, the experimentally determined 20S proteome has an increased interaction capacity [15], which potentially regulates the degradation by the 20S proteasome. Although individual examples, where complexation extends protein half-life (e.g. iκBα- NFκB [21], Ku70-Ku80 [22]) have been documented, the detailed molecular mechanisms remained to be elucidated.

We used the activator protein 1 (AP-1) model system to study the relationship between protein interactions and half-life. AP-1 regulates a number of cellular processes including differentiation, proliferation, and apoptosis via controlling gene expression in response to a plethora of signals, including cytokines, growth factors, stress, and viral infections [23]. AP-1 is a heterodimer, which is composed of proteins belonging to the c-Fos and c-Jun families [24]. The c-Fos transcription factor has a short half-life [25], which could be elongated by its partner, c-Jun as well as by the 20S proteasome 'gatekeeper' NQO1 [26, 27]. Multiple evidence demonstrates that c-Fos is degraded by different mechanisms, also independently from ubiquitination [28-30]. Here we investigated how c-Fos turnover is modulated by specific mutations at contact sites with c-Jun and by the presence of the unstructured tail. Our results demonstrate that both specific and transient, nonspecific interactions influence half-life and propose a mechanism to regulate protein degradation via fine-tuning the interaction affinities with a binding partner.

Results

Mutant design. The structure of the AP-1 complex is a coiled-coil (PDB code: 1fos, [31]), which is held together by interdigitating hydrophobic contacts ('leucine zipper'). These are complemented by salt bridges at specific positions, which stabilize heterodimers as compared to homodimers. We designed five mutants using the full-length c-Fos: two affecting the hydrophobic network (L165V, L172V), and three perturbing the hydrophilic contacts (E175D, E189D, K190R) (Figure 1A). In case of L $\rightarrow$ V and E $\rightarrow$ D replacements, the smaller sidechains might cause deviations from the ideal geometry, while maintaining the polarity of the interaction. The K $\rightarrow$ R mutation introduces a bulkier sidechain with additional π interactions. The C-terminal region of c-Fos comprises three PEST sequences [32], which do not overlap with the designed mutations.

The crystal structure comprises only those segments of c-Fos and c-Jun (139-200 aa c-Fos and 263-324 aa c-Jun), which adopt a well-defined helical structure upon binding [31]. The C-terminal region of c-Fos however, dynamically fluctuates amongst various conformations both in the free form [33] as well as bound to c-Jun [34]. This mode of assembly, with extensive conformational exchange upon partner interactions, is referred to as a fuzzy complex [35, 36]. We also designed a truncation mutant (c-Fos$_{\Delta 214}$) to probe the effect of the fuzzy C-terminal tail of c-Fos (215-380 AA).

c-Fos forms a fuzzy complex with c-Jun. We applied electronic circular dichroism (ECD) spectroscopy to assess the impact of the mutations on c-Fos structure in the free form as well as in complex with full-length c-Jun (Table S1). In accord with previous experimental results, almost half of the residues in c-Fos (185 out of 380 AA) do not possess regular secondary structures and are disordered [33]. Interaction with c-Jun slightly increases the helical population of c-Fos as compared to the free state, but does not induce extensive ordering (Table 1). These data indicate that c-Fos forms a fuzzy complex with c-Jun, where 45.8 % of the residues remain to be disordered, consistently with previous FRET and FCCS results [34]. On the other hand, no substantial unfolding of the structured part takes place, as the number of residues with regular secondary conformations (> 200 AA in full-length c-Fos, 113 AA in c-Fos$_{\Delta 214}$) exceeds the size of the bHLH/LZ (62 AA). The L172V and E175D substitutions cause only minor increase in the secondary structures of c-Fos (Table 1). Structural disorder of the c-Fos$_{L172V}$ and c-Fos$_{L175D}$ mutants is retained upon assembly with c-Jun, with small impact on the secondary structure properties as compared to the wild-type protein. Secondary structure predictions by the GOR IV algorithm [37] suggest a considerable reduction in helicity in c-Fos$_{L165V}$ as compared to the wild type protein or c-Fos$_{L172V}$ (Table S2).

Deletion of the disordered C-terminal region (215-380 AA) has a negligible impact on c-Fos structure (Table 1). This is due to the removal of only 166 out of 323 disordered residues. The remaining unstructured fraction also includes a 15-residue disordered segment flanking the leucine zipper (200-214 AA), which reduces termination effects. Interactions with full-length c-Jun have a moderate influence on the secondary structure properties of c-Fos$_{\Delta 214}$. Taken together, c-Fos and all the studied variants form a fuzzy complex with c-Jun and do not completely fold upon binding.

Both specific and fuzzy interactions modulate binding affinity. To assess the effect of binding affinity on the degradation rate of c-Fos, specific contacts between c-Fos/c-Jun complex were perturbed (Figure 1A). In contrast to most previous studies (Table S3 and references therein), we used the full-length c-Fos (380 AA) and c-Jun (331 AA) to investigate the interplay between the specific interactions by the structured elements and the transient interactions by the fuzzy tail. All substitutions decrease binding affinity by less than two orders of magnitude, except the K190R mutation (Table 2). Perturbing the hydrophobic interface (L165V, L172V) has the most considerable effect on the stability of the complex due to looser zipper contacts. Reducing the size of the negatively charged residues (E175D, E189D) has a moderate impact on K_D, due to weaker electrostatic interactions. The K190R mutation slightly stabilizes the heterodimer via additional π- π interactions with Q313. Mutations in full-length c-Fos mostly affect the association kinetics, in line with previous data [38, 39].

Binding of full-length proteins without complete folding might exhibit complex kinetics [40, 41] (and references therein), as compared to protein fragments, which become structured upon binding [42]. Therefore, inclusion of the fuzzy tails in full-length c-Fos (380 AA) and c-Jun (331 AA) improves binding affinity (40 nM, Table 2) as compared to the interactions between leucine zippers (63 AA, K_D=54nM, [43]). Indeed, removal of the disordered tail in c-Fos$_{\Delta 214}$ considerably destabilizes the dimer (Table 2). A similar trend has been observed in c-Max and c-Myc assembly, where the fuzzy tail masks the electrostatic repulsion between the coiled-coil regions [44, 45].

Within the framework of the fly-casting model, disordered regions increase local concentration nearby the target via nonspecific (e.g. electrostatic) interactions [46, 47]. Along these lines fuzzy regions in protein complexes can serve as nonspecific anchors, which remain attached and decrease dissociation rates even in the absence of specific contacts [36]. Indeed, the removal of the fuzzy C-terminal region in c-Fos$_{\Delta 214}$ considerably increases the dissociation rate from c-Jun as compared to the wild-type protein (Table 2). Replacements of charged residues in full-length c-Fos also slow down the dissociation rates by 3-4 folds (Table 2), consistently with the fly-casting model. The more complex kinetics is also illustrated in case of the c-Fos$_{L165V}$ and c-Fos$_{L172V}$ mutants, where data could be fitted better using a 2-state model (Table S4).

We also determined the changes in interaction energies ($\Delta\Delta \boldsymbol{G}_{\boldsymbol{int}}^{\boldsymbol{wt}\rightarrow\boldsymbol{mut}}$) using the FoldX program [48] based on the coiled-coil structure (1fos.pdb [31]). Although the computed $\Delta\Delta \boldsymbol{G}_{\boldsymbol{int}}^{\boldsymbol{wt}\rightarrow\boldsymbol{mut}}$ results qualitatively reproduce the experimental trends (i.e. the K190R mutation is stabilizing, the L $\rightarrow$ V mutations at the helix-helix interface are destabilizing), they are considerably smaller than those deduced from the experimental binding affinities of the full models. These results corroborate the interactions between fuzzy tail and the helical interface.

Changes in c-Fos degradation rates correlate to interaction strength. c-Fos is degraded via both ubiquitination and ubiquitin-independent mechanisms [25]. The disordered regions can contribute to both pathways [49], out of which the 'default' degradation mechanism mediated by the 20S proteasome was addressed [16, 26]. Using a purified proteasome assay [50, 51], we followed c-Fos degradation in the absence and presence of c-Jun. The E $\rightarrow$ D replacements stabilize the free c-Fos, whereas the K190R and Δ214 shorten c-Fos half-life. The initial degradation rates of free c-Fos however, are not affected considerably by the site-specific mutations or C-terminal truncation (Table 3), consistently with moderate change in c-Fos structure (Table 1, Table S1). These results indicate that the mutations do not alter interactions with the 20S proteasome and changes in c-Fos degradation are due to the partnership with c-Jun.

Interactions with c-Jun impair c-Fos degradation by the 20S proteasome, in accord with previous results [26]. All the mutations have a larger impact on c-Fos half-life in the presence than in the absence of c-Jun, indicating that interactions with the binding partner influence c-Fos degradation (Table 3). c-Fos turnover is prolonged in all cases, independently whether the mutation stabilize or destabilize the complex ($v_{+c\text{-}Jun}/v_{free}$ < 1, Table 3). The impact on the initial degradation rates however, parallels the interaction strength of the mutant (Table 3, Figure 1B). Destabilizing the complex reduces the protecting role of the binding partner as compared to the wild-type. In accord, the destabilizing L172V mutation, which affects

hydrophobic contacts exhibits smaller decrease in the initial degradation rates than those affecting hydrophilic interactions (E175D, E189D). In contrast, the stabilizing K190R mutation slows down the initial degradation as compared to the wild-type c-Fos (Figure 1B). The c-Fos$_{L165V}$ however, exhibits substantial deviation from these trends, owing to its considerably decreased helicity (Table S2) and decreased dissociation rates (Table 2).

The presence of the c-Fos fuzzy tail also decreases the degradation rate almost by 4-fold (Table 3), consistently with its significant contribution to the stability of the AP-1 complex (Table 2). Thus, removal of the fuzzy C-terminal segment decreases c-Fos protection via weakening the complexation with c-Jun (Table 3). Taken together, although interaction affinity is likely to be the major determinant in stabilizing c-Fos, the relationship appears to be rather complex.

Discussion

The nanny hypothesis provides a plausible model for how regulatory regions, which do not adopt a folded structure can survive degradation by the 20S proteasome machinery [20]. This model is particularly relevant for proteins with intrinsically disordered regions [52], which constitute about one third of the human proteome [53]. Although structural data indicate the lack of a compact structure also in vivo [54], persistence of this feature challenges the quality control mechanisms of the cell. A possible solution is to link the expression of an ID protein to an interacting partner, which can mask and thus protect the fluctuating, unfolded segment from degradation [20]. This may drive protein assembly in vivo [21, 22], molecular details of which have remained to be enigmatic.

Here we aimed to explore how specificity and affinity of protein interactions influence degradation by the 20S proteasome. Using the AP-1 as a model system, we demonstrated that both hydrophobic and hydrophilic contacts at the helix-helix interface affect c-Fos degradation. We also showed that protection by the partner qualitatively correlates to the binding affinity; and destabilizing the assembly reduces the impact of the mutation on degradation rates. There are additional factors however, which can also influence stabilization, for example decreased dissociation rates, or steric effects (in larger systems, not studied here) indicating a rather complex protection mechanism. Taken together, these results suggest that protein turnover can be modulated via fine-tuning the association with a binding partner.

ECD measurements evidence that the C-terminal tail of c-Fos retains its disordered state in complex with c-Jun. This supports that protection of disordered regions can be achieved without inducing a stable structure and many binding configurations could be visited in the bound-state without decreasing the conformational entropy [36]. Thus, 20S proteasome degradation can be impaired via a fuzzy assembly between the nanny and its client(s) and may not require specific chaperones [55]. Consequently, fine-tuning the dynamics of fuzzy regions, e.g. via post-translational modifications could significantly affect half-life [56, 57].

The protective role of fuzzy interactions from the 20S proteasome could also provide a plausible explanation for how low-complexity sequence motifs might serve as selective inhibitors of proteolysis [13, 14]. Tandem repeats of short, linear sequences are frequently associated with proteins, which form higher-order protein structures or undergo liquid-liquid

phase transition [58]. Interactions between these motifs is often not specific or well-defined, and multivalency [59] or fuzziness [60] is a ubiquitous feature of these associations. We may assume that such weak, heterogeneous contacts could also serve to protect disordered stretches with multivalent, low-complexity motifs [61] from the ubiquitin independent degradation pathway.

Conclusion

Our work highlight a novel aspect of protein fuzziness in regulating of protein half-life. First, we demonstrate that protection of disordered regions from degradation could be achieved without inducing a stable structure. Binding to a partner generates a fuzzy complex, where significant conformational entropy is retained. Second, we show that both specific contacts and fuzzy interactions can impair protein degradation, proportionally to their contribution to binding affinity; suggesting that protein turnover can be regulated via fine-tuning protein assembly. Third, low-complexity motifs may selectively inhibit proteolysis by generating higher-order structures via fuzzy interactions, suggesting the role of membraneless cellular compartments in protecting disordered regions from degradation. Investigating this aspect of the model is ongoing in our laboratory.

Acknowledgement

We are indebted to Jörg Langowski (DKFZ, Heidelberg) for providing the Fos-EGFP and Jun-mRFP1 constructs in 2013, which have been used in our preliminary studies. Owing to his tragic accident in 2017, we dedicate the article to his memory. We also thank Krisztina Tar, Zsolt Bacsó and György Vámosi for fruitful discussions and Barbara Sárkány for careful reading of the manuscript. The 2-state model binding kinetics were evaluated by Bálint Bécsi. Financial support is provided by GINOP-2.3.2-15-2016-00044, HAS 11015 and the DE Excellence Program (M.F.). T. K. and S. B. K. thank the National Research, Development and Innovation Office (NKFI K120181) for financial support.

References

[1] Hershko A, Ciechanover A. The ubiquitin system. Annu Rev Biochem. 1998;67:425-79.
[2] Voges D, Zwickl P, Baumeister W. The 26S proteasome: a molecular machine designed for controlled proteolysis. Annu Rev Biochem. 1999;68:1015-68.
[3] Pagano M, Tam SW, Theodoras AM, Beer-Romero P, Del Sal G, Chau V, et al. Role of the ubiquitin-proteasome pathway in regulating abundance of the cyclin-dependent kinase inhibitor p27. Science. 1995;269:682-5.
[4] Hoeller D, Dikic I. Targeting the ubiquitin system in cancer therapy. Nature. 2009;458:438-44.
[5] Ciechanover A. Intracellular protein degradation: From a vague idea thru the lysosome and the ubiquitin-proteasome system and onto human diseases and drug targeting. Biochim Biophys Acta. 2011;1824:3-13.
[6] Huang X, Luan B, Wu J, Shi Y. An atomic structure of the human 26S proteasome. Nat Struct Mol Biol. 2016;23:778-85.
[7] da Fonseca PC, Morris EP. Cryo-EM reveals the conformation of a substrate analogue in the human 20S proteasome core. Nature communications. 2015;6:7573.
[8] Chen P, Hochstrasser M. Autocatalytic subunit processing couples active site formation in the 20S proteasome to completion of assembly. Cell. 1996;86:961-72.
[9] Prakash S, Tian L, Ratliff KS, Lehotzky RE, Matouschek A. An unstructured initiation site is required for efficient proteasome-mediated degradation. Nat Struct Mol Biol. 2004;11:830-7.
[10] Ravid T, Hochstrasser M. Diversity of degradation signals in the ubiquitin-proteasome system. Nat Rev Mol Cell Biol. 2008;9:679-90.
[11] Prakash S, Inobe T, Hatch AJ, Matouschek A. Substrate selection by the proteasome during degradation of protein complexes. Nat Chem Biol. 2009;5:29-36.
[12] Fishbain S, Inobe T, Israeli E, Chavali S, Yu H, Kago G, et al. Sequence composition of disordered regions fine-tunes protein half-life. Nat Struct Mol Biol. 2015;22:214-21.
[13] Sharipo A, Imreh M, Leonchiks A, Imreh S, Masucci MG. A minimal glycine-alanine repeat prevents the interaction of ubiquitinated I kappaB alpha with the proteasome: a new mechanism for selective inhibition of proteolysis. Nat Med. 1998;4:939-44.
[14] Yu H, Singh Gautam AK, Wilmington SR, Wylie D, Martinez-Fonts K, Kago G, et al. Conserved Sequence Preferences Contribute to Substrate Recognition by the Proteasome. J Biol Chem. 2016;291:14526-39.
[15] Myers N, Olender T, Savidor A, Levin Y, Reuven N, Shaul Y. The Disordered Landscape of the 20S Proteasome Substrates Reveals Tight Association with Phase Separated Granules. Proteomics. 2018;18:e1800076.
[16] Asher G, Reuven N, Shaul Y. 20S proteasomes and protein degradation "by default". Bioessays. 2006;28:844-9.
[17] van der Lee R, Lang B, Kruse K, Gsponer J, Sanchez de Groot N, Huynen MA, et al. Intrinsically disordered segments affect protein half-life in the cell and during evolution. Cell reports. 2014;8:1832-44.
[18] Asher G, Bercovich Z, Tsvetkov P, Shaul Y, Kahana C. 20S proteasomal degradation of ornithine decarboxylase is regulated by NQO1. Mol Cell. 2005;17:645-55.
[19] Moscovitz O, Tsvetkov P, Hazan N, Michaelevski I, Keisar H, Ben-Nissan G, et al. A mutually inhibitory feedback loop between the 20S proteasome and its regulator, NQO1. Mol Cell. 2012;47:76-86.

[20] Tsvetkov P, Reuven N, Shaul Y. The nanny model for IDPs. Nat Chem Biol. 2009;5:778-81.
[21] Krappman D, Wulczyn FG, Scheidereit C. Different mechanisms control signal induced degradation and basal turnover of the NF-kappaB inhibitor and inhibitor ikappaB alpha in vivo. EMBO J. 1996;15:6716-26.
[22] Gu Y, Seidl KJ, Rathbun GA, Zhu C, Manis JP, van der Stoep N, et al. Growth retardation and leaky SCID phenotype of Ku70-deficient mice. Immunity. 1997;7:653-65.
[23] Eferl R, Wagner EF. AP-1: a double-edged sword in tumorigenesis. Nat Rev Cancer. 2003;3:859-68.
[24] Chinenov Y, Kerppola TK. Close encounters of many kinds: Fos-Jun interactions that mediate transcription regulatory specificity. Oncogene. 2001;20:2438-52.
[25] Bossis G, Ferrara P, Acquaviva C, Jariel-Encontre I, Piechaczyk M. c-Fos proto-oncoprotein is degraded by the proteasome independently of its own ubiquitinylation in vivo. Mol Cell Biol. 2003;23:7425-36.
[26] Adler J, Reuven N, Kahana C, Shaul Y. c-Fos proteasomal degradation is activated by a default mechanism, and its regulation by NAD(P)H:quinone oxidoreductase 1 determines c-Fos serum response kinetics. Mol Cell Biol. 2010;30:3767-78.
[27] Tsvetkov P, Myers N, Moscovitz O, Sharon M, Prilusky J, Shaul Y. Thermo-resistant intrinsically disordered proteins are efficient 20S proteasome substrates. Mol Biosyst. 2012;8:368-73.
[28] Acquaviva C, Salvat C, Brockly F, Bossis G, Ferrara P, Piechaczyk M, et al. Cellular and viral Fos proteins are degraded by different proteolytic systems. Oncogene. 2001;20:942-50.
[29] Jariel-Encontre I, Pariat M, Martin F, Carillo S, Salvat C, Piechaczyk M. Ubiquitinylation is not an absolute requirement for degradation of c-Jun protein by the 26 S proteasome. J Biol Chem. 1995;270:11623-7.
[30] Jariel-Encontre I, Salvat C, Steff AM, Pariat M, Acquaviva C, Furstoss O, et al. Complex mechanisms for c-fos and c-jun degradation. Mol Biol Rep. 1997;24:51-6.
[31] Glover JN, Harrison SC. Crystal structure of the heterodimeric bZIP transcription factor c-Fos-c-Jun bound to DNA. Nature. 1995;373:257-61.
[32] Rechsteiner M, Rogers SW. PEST sequences and regulation by proteolysis. Trends Biochem Sci. 1996;21:267-71.
[33] Campbell KM, Terrell AR, Laybourn PJ, Lumb KJ. Intrinsic structural disorder of the C-terminal activation domain from the bZIP transcription factor Fos. Biochemistry. 2000;39:2708-13.
[34] Vamosi G, Baudendistel N, von der Lieth CW, Szaloki N, Mocsar G, Muller G, et al. Conformation of the c-Fos/c-Jun complex in vivo: a combined FRET, FCCS, and MD-modeling study. Biophys J. 2008;94:2859-68.
[35] Fuxreiter M. Fuzziness in Protein Interactions-A Historical Perspective. J Mol Biol. 2018;430:2278-87.
[36] Fuxreiter M. Fold or not to fold upon binding - does it really matter? Current Opinion in Structural Biology. 2018;54:19-25.
[37] Garnier J, Gibrat J-F, Robson B. GOR secondary structure prediction method version IV. Methods Enzymol1996. p. 540-53.
[38] Dogan J, Gianni S, Jemth P. The binding mechanisms of intrinsically disordered proteins. Phys Chem Chem Phys. 2014;16:6323-31.
[39] Gianni S, Dogan J, Jemth P. Coupled binding and folding of intrinsically disordered proteins: what can we learn from kinetics? Curr Opin Struct Biol. 2016;36:18-24.

[40] Berlow RB, Dyson HJ, Wright PE. Hypersensitive termination of the hypoxic response by a disordered protein switch. Nature. 2017;543:447-51.
[41] Miskei M, Antal C, Fuxreiter M. FuzDB: database of fuzzy complexes, a tool to develop stochastic structure-function relationships for protein complexes and higher-order assemblies. Nucleic Acids Res. 2017;45:D228-D35.
[42] Shammas SL, Crabtree MD, Dahal L, Wicky BI, Clarke J. Insights into Coupled Folding and Binding Mechanisms from Kinetic Studies. J Biol Chem. 2016;291:6689-95.
[43] Kohler JJ, Schepartz A. Kinetic studies of Fos.Jun.DNA complex formation: DNA binding prior to dimerization. Biochemistry. 2001;40:130-42.
[44] Pursglove SE, Fladvad M, Bellanda M, Moshref A, Henriksson M, Carey J, et al. Biophysical properties of regions flanking the bHLH-Zip motif in the p22 Max protein. Biochem Biophys Res Commun. 2004;323:750-9.
[45] Naud JF, McDuff FO, Sauve S, Montagne M, Webb BA, Smith SP, et al. Structural and thermodynamical characterization of the complete p21 gene product of Max. Biochemistry. 2005;44:12746-58.
[46] Shoemaker BA, Portman JJ, Wolynes PG. Speeding molecular recognition by using the folding funnel: the fly-casting mechanism. Proc Natl Acad Sci U S A. 2000;97:8868-73.
[47] Huang Y, Liu Z. Kinetic advantage of intrinsically disordered proteins in coupled folding-binding process: a critical assessment of the "fly-casting" mechanism. J Mol Biol. 2009;393:1143-59.
[48] Schymkowitz J, Borg J, Stricher F, Nys R, Rousseau F, Serrano L. The FoldX web server: an online force field. Nucleic Acids Res. 2005;33:W382-8.
[49] Guharoy M, Bhowmick P, Sallam M, Tompa P. Tripartite degrons confer diversity and specificity on regulated protein degradation in the ubiquitin-proteasome system. Nature communications. 2016;7:10239.
[50] Tar K, Dange T, Yang C, Yao Y, Bulteau AL, Salcedo EF, et al. Proteasomes associated with the Blm10 activator protein antagonize mitochondrial fission through degradation of the fission protein Dnm1. J Biol Chem. 2014;289:12145-56.
[51] Bhattacharyya S, Renn JP, Yu H, Marko JF, Matouschek A. An assay for 26S proteasome activity based on fluorescence anisotropy measurements of dye-labeled protein substrates. Anal Biochem. 2016;509:50-9.
[52] Dyson HJ, Wright PE. Intrinsically unstructured proteins and their functions. Nat Rev Mol Cell Biol. 2005;6:197-208.
[53] Ward JJ, Sodhi JS, McGuffin LJ, Buxton BF, Jones DT. Prediction and functional analysis of native disorder in proteins from the three kingdoms of life. J Mol Biol. 2004;337:635-45.
[54] Theillet FX, Binolfi A, Bekei B, Martorana A, Rose HM, Stuiver M, et al. Structural disorder of monomeric alpha-synuclein persists in mammalian cells. Nature. 2016;530:45-50.
[55] Hartl FU. Unfolding the chaperone story. Mol Biol Cell. 2017;28:2919-23.
[56] Andresen C, Helander S, Lemak A, Fares C, Csizmok V, Carlsson J, et al. Transient structure and dynamics in the disordered c-Myc transactivation domain affect Bin1 binding. Nucleic Acids Res. 2012;40:6353-66.
[57] Helander S, Montecchio M, Pilstal R, Su Y, Kuruvilla J, Elven M, et al. Pre-Anchoring of Pin1 to Unphosphorylated c-Myc in a Fuzzy Complex Regulates c-Myc Activity. Structure. 2015;23:2267-79.
[58] Boeynaems S, Alberti S, Fawzi NL, Mittag T, Polymenidou M, Rousseau F, et al. Protein Phase Separation: A New Phase in Cell Biology. Trends Cell Biol. 2018;28:420-35.

[59] Li P, Banjade S, Cheng HC, Kim S, Chen B, Guo L, et al. Phase transitions in the assembly of multivalent signalling proteins. Nature. 2012;483:336-40.
[60] Wu H, Fuxreiter M. The Structure and Dynamics of Higher-Order Assemblies: Amyloids, Signalosomes, and Granules. Cell. 2016;165:1055-66.
[61] Burke KA, Janke AM, Rhine CL, Fawzi NL. Residue-by-Residue View of In Vitro FUS Granules that Bind the C-Terminal Domain of RNA Polymerase II. Mol Cell. 2015;60:231-41.
[62] Sultana A, Lee JE. Measuring protein-protein and protein-nucleic Acid interactions by biolayer interferometry. Curr Protoc Protein Sci. 2015;79:19 25 1-6.

Figure legend

Figure 1 (A) Designed mutations in the structure of the AP-1 complex (1.fos.pdb [31]). Mutations in c-Fos (marine, black labels) and the contacting residues in c-Jun (cyan, grey labels) are shown by spheres. Fuzzy C-terminal tails are displayed by dashed lines, the DNA is colored grey. **(B)** Change in c-Fos degradation rate via c-Jun interactions ($v_{+c\text{-}Jun}/v_{free}$) as a function of the binding affinity. The experimental K_D values are shown on a logarithmic scale.

MATERIALS AND METHODS

Protein expression and purification

The coding sequences of human c-Fos (Uniprot: P01100), c-Fos$_{\Delta 214}$, c-Jun (donated by Joerg Langowski, DKFZ in Heidelberg, Germany [34]) were cloned into the pET-Duet-1 vector. Site-directed mutagenesis was carried out by the QuikChange II Site-Directed Mutagenesis Kit (Agilent Technologies). Proteins were expressed in *E. coli* bacterial cultures (Rosetta2(DE3)pLysS, Novagen) using IPTG induction for 3 hours. Proteins purification was performed by immobilized metal affinity chromatography using a Ni-Sepharose™ 6 Fast Flow resin (GE Healthcare) with a lysis buffer containing 250 mM imidazole. Proteins were dialyzed against 100 volumes of 4M, 2M and 1M urea consecutively, then the buffer was changed to 25 mM Tris-HCl, pH7.4, 100 mM NaCl. The eluted proteins were concentrated with an Amicon-Ultra 50 10000 MWCO ultrafiltration device. Protein concentrations were determined by BCA protein assay.

Determination of binding kinetics

The binding kinetics of c-Fos variants to c-Jun were measured with a BLItz (PALL-ForteBio) biolayer interferometer [62]. 1.5 µg of c- Jun was pre-complexed with 60A8 anti-Jun antibody (Cell Signaling Technologies) at 37°C until saturation has been reached. The antibody does not compete with c-Jun for binding to c-Fos (c-Jun does not significantly reduce the signal intensity of 6A9 Ab in the ELISA assay, see below) and is not specific to the C-terminus (it can also detect the c-Fos$_{\Delta 214}$ variant). The complex was loaded onto Protein-A Dip and Read biosensors to a spectral shift of 3.5 nm. c-Fos variants were diluted into PBS containing 0.1% Tween-20 to various concentrations and their association to c-Jun was measured before the biosensor was dipped into the same buffer to record the dissociation of the proteins. The binding curves were fitted to a 1:1 binding model using the BLItz Pro™ software.

In vitro 20S proteasome assay

c-Fos variants and human 20S proteasome (Boston Biochem, Cat.# E-360) were diluted in solution of 25 mM Tris-HCl (pH7.5), 100 mM NaCl, 0.5 mM DTT to concentrations of 400 nM (c-Fos) and 8 nM (20S proteasome). The degradation assay was performed by mixing 12.5 µl of each solution. Degradation of the c-Fos was followed at 37°C and 2 µl samples were collected at 0, 15, 40 and 80 minutes, which were transferred into a solution containing 98 µl of PBS, 0.1% Tween-20, 1% BSA, 1 µM PS341 and protease inhibitors (EDTA free protease inhibitor coctail, Roche). The amount of c-Fos at each time point was determined using an ELISA assay. The c-Fos solution was loaded onto 96-well Pierce Nickel-coated plates (Thermo Scientific, cat.# 15442) at 25 °C. After 1 hour, the wells were washed with PBS-0.1% Tween-20 three times and 9F6 anti-cFos antibody (Cell Signaling Technologies, 0.002 dilution) was added. This was followed by a reaction with HRP-conjugated anti-rabbit IgG (1:1000) and

tetramethyl-benzidine (Sigma, T4444). The reaction was terminated by 1M HCl and intensity was measured at λ=450 nm using Synergy H1 microplate reader (BioTeK Instruments). Protein amounts were computed based on a calibration curve obtained with BSA-determined concentrations. Nonlinear fitting of the decay curves was performed by the R program, using a 1:1 binding model. All reactions were run in triplicates.

Table 1. Propensity of unstructured secondary structure elements (%) as determined by ECD spectroscopy. ECD spectra were recorded on a J-810 spectropolarimeter in 20 mM sodium phosphate, pH 7.4 buffer solution with a 0.2 mm quartz cell at room temperature. Raw spectra were corrected with the blank, then were converted to mean residue ellipticities and were smoothed. Deconvolution was performed by the BeStSel program [53, 54].

	Unstructured (%)	
	free	**+ c-Jun**
c-Fos	48.7	44.2
c-Jun	44.4	–
c-Fos$_{L172V}$	44.5	42.5
c-Fos$_{E175D}$	42.1	46.5
c-Fos$_{\Delta 214}$	46.2	47.1

Table 2. Experimental binding affinities and computed interaction energies of c-Fos mutants with c-Jun. Association and dissociation curves were determined at 37 °C by BLItz analysis [55] using a 1:1 binding model. c-Fos mutants were added to Jun labelled biosensors in different concentrations. Jun was marked by 60A8 Jun antibody (Cell Signaling Technologies). The equilibrium dissociation constant was determined as $K_D=k_d/k_a$, where k_d is the dissociation, k_a is the association rate. $\Delta\Delta G_{int}^{wt\rightarrow mut}$ was computed by the FoldX program [41]. Amino acid replacements were carried out on the 1fos.pdb structure [31] and mutated residues were subjected to short relaxation. As the fuzzy C-terminal tail of c-Fos was not included, the changes in interaction energy between the structured segments were computed.

	k_a (x10^3 $M^{-1}s^{-1}$)	k_d (x10^4 s^{-1})	K_D (nM)	affinity ratio to wild type	$\Delta\Delta G_{int}^{wt\rightarrow mut}$ (kcal/mol)
c-Fos	80.3 ± 18.5	32.4 ± 1.95	40.4 ± 22.6	–	–
c-Fos$_{L165V}$	1.82 ± 0.0337	23.8 ± 0.897	1310 ± 73.8	0.03	0.77
c-Fos$_{L172V}$	8.16 ± 0.197	55.1 ± 2.28	676 ± 79.7	0.06	1.51
c-Fos$_{E175D}$	7.76 ± 0.119	11.6 ± 0.738	149 ± 85.3	0.27	0.01
c-Fos$_{E189D}$	5.53 ± 0.0637	7.02 ± 0.474	127 ± 125	0.32	-0.01
c-Fos$_{K190R}$	76.4 ± 0.876	7.75 ± 0.481	10.1 ± 5.79	4.0	-0.17
c-Fos$_{\Delta 214}$	3.11 ± 0.421	77.8 ± 1.44	2500 ± 511	0.02	–

Table 3. Half-lifes and initial degradation rates of c-Fos in the absence and in the presence of c-Jun. Degradation assays have been performed using purified human 20S proteasomes [43] by measuring c-Fos concentration at 0, 15, 40 and 80 minutes. Initial degradation rates were obtained by nonlinear data fitting of the decay curves using the R program. All reactions were run in triplicates. $v_{+c\text{-}Jun}/v_{free}$ is the ratio of the initial degradation rates of c-Fos in the complex and the free form.

	Half-life (min)		**Initial degradation rate (O.D./min)**		
	free	**+ c-Jun**	**free (x 10^{-2})**	**+ c-Jun (x 10^{-2})**	**$v_{+c\text{-}Jun}/v_{free}$**
c-Fos	11.64 ± 0.44	19.18 ± 9.00	3.00 ± 0.14	0.74 ± 0.60	0.247
c-Fos$_{L165V}$	10.84 ± 0.13	14.16 ± 3.74	3.46 ± 0.04	1.01 ± 0.22	0.292
c-Fos$_{L172V}$	10.93 ± 3.53	15.69 ± 2.76	3.31 ± 0.77	1.98 ± 0.46	0.598
c-Fos$_{E175D}$	23.95 ± 2.35	23.67 ± 7.90	3.08 ± 0.18	1.29 ± 0.30	0.419
c-Fos$_{E189D}$	17.36 ± 1.15	20.73 ± 2.32	3.07 ± 0.09	1.46 ± 0.66	0.476
c-Fos$_{K190R}$	9.28 ± 2.86	151.95 ± 33.87	2.46 ± 0.72	0.24 ± 0.08	0.097
c-Fos$_{\Delta 214}$	9.07 ± 1.25	13.85 ± 4.09	2.86 ± 0.48	2.69 ± 0.48	0.941

Figure

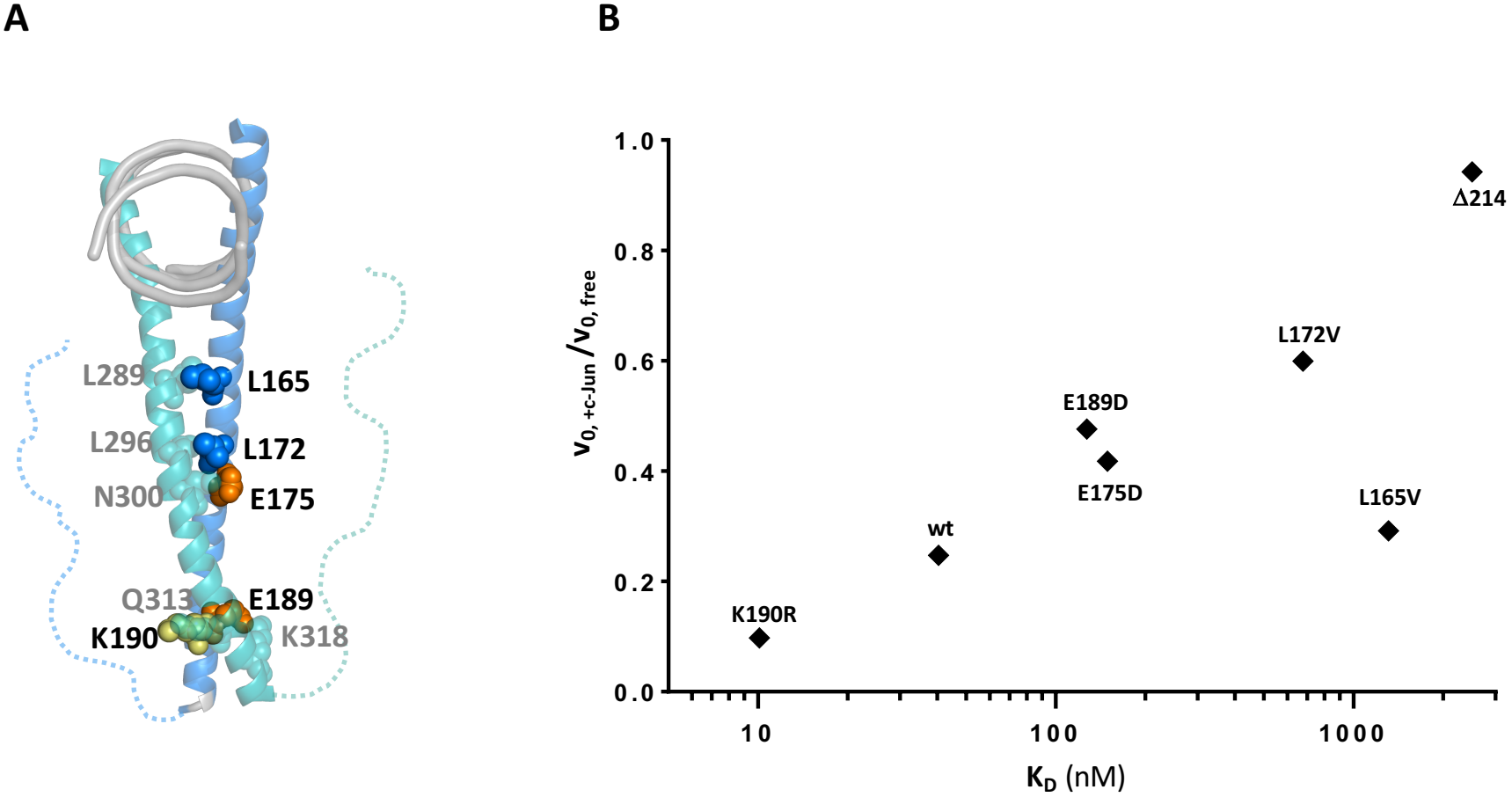
A
L289
L165
L296
L172
N300
E175
Q313
E189
K190
K318
B
1.0
0.8
0.6
0.4
0.2
0.0
$v_{0,\ +c\text{-}Jun}/v_{0,\ free}$
Δ214
L172V
E189D
E175D
L165V
wt
K190R
10
100
1000
K_D (nM)

Electronic Supplementary Material (online publication only)

Click here to download Electronic Supplementary Material (online publication only): halflife_table_suppl.pdf